

# Current ripple reduction for finite control set model predictive control strategy of grid-tied inverter with reference current compensation

NAN JIN , WUCHUANG FAN, JIE FANG , JIE WU, YONGPENG SHEN

*Zhengzhou University of Light Industry  
College of Electrical and Information Engineering  
China*

*e-mail: fang0511jie@126.com*

(Received: 07.06.2022, revised: 26.09.2022)

**Abstract:** In the finite control set model predictive control (FCS-MPC) strategy of the grid-tied inverter, the current ripple (CR) affects the selection of optimal voltage vectors, which leads to the increase of output current ripples. In order to solve this problem, this paper proposes a CR reduction method based on reference current compensation (RCC) for the FCS-MPC strategy of grid-tied inverters. Firstly, the influence of the CR on optimal voltage vector selection is analyzed. The conventional CR prediction method is improved, which uses inverter output voltage and grid voltage to calculate current ripples based on the space state equation. It makes up for the shortcomings that the conventional CR prediction method cannot predict in some switching states. The improved CR method is more suitable for the FCS-MPC strategy. In addition, the differences between the two cost functions are compared through visual analysis. It is found that the sensitivity of the square cost function to small errors is better than that of the absolute value function. Finally, the predicted CR is used to compensate the reference current. The compensated reference current is substituted into the square cost function to reduce the CR. The experimental results show that the proposed method reduces the CR by 47.3%. The total harmonic distortion (THD) of output current is reduced from 3.86% to 2.96%.

**Key words:** cost function, current ripple reduction, finite control set model predictive control (FCS-MPC), grid-tied inverter, reference current compensation (RCC)



## Nomenclature

Symbol	Implication	Symbol	Implication
CR	Current ripple	$g_1$	Type A cost function
RCC	Reference current compensation	$g_2$	Type B cost function
VSI	Voltage source inverter	$\nabla g_1$	Gradient of $g_1$
$u_{abc}$	Output voltage	$\nabla g_2$	Gradient of $g_2$
$e_{abc}$	Grid voltage	$\delta$	Cost function error
$i_{abc}$	Output current	$i_{\alpha\beta\_com}^*$	Compensated reference current
$U_{dc}$	DC voltage	$i_{\alpha\beta\_rip}^P$	Predictive current ripple
$L$	Filter inductance	$d$	Voltage vector duration
$R$	Stray resistance	$u_m$	Modulation amplitude
$i_{\alpha\beta}^P$	Predictive current	$U_{tri}$	Triangular carrier amplitude
$i_{\alpha\beta}^*$	Reference current	$\Delta i_L$	Inverter output current error
$\Delta u$	Inductance fluctuating voltage	$X(k)$	Value of $X$ at $(k)$ -th instant
$T$	Control period	$X(k+1)$	Value of $X$ at $(k+1)$ -th instant

## 1. Introduction

With the increasing scale of renewable energy represented by photovoltaic and wind energy in the modern power system, the requirements for the efficiency and reliability of grid-tied inverters are gradually improved [1]. Three-phase inverters were widely used in renewable energy power generation [2–4]. As a connection between renewable energy and the power grid, the output current of inverters controlled by conventional finite control set model predictive control (FCS-MPC) causes a large ripple due to the limitation of the switching frequency. The current ripple (CR) affects the selection of the optimal voltage vector at the  $(k+1)$ -th instant so that the optimal voltage vector is inaccurately selected. Eventually, it reduces the performance of grid-tied inverters. With the high penetration of large-scale renewable energy into the grid, the stability of the grid was reduced. Therefore, it is necessary to improve the FCS-MPC strategy.

The CR of grid-tied inverters is one of the main factors for the total harmonic distortion (THD) of grid-tied inverter output current. The FCS-MPC strategy of voltage source inverters (VSI) [5–9] has been studied. The optimal voltage vector is selected by comparing the predicted value and the reference value without pulse width modulation (PWM), phase-locked loop (PLL) and other controllers. For the FCS-MPC strategy, only one voltage vector is applied during a switching period. The CR can be reduced by increasing the switching frequency. However, it will lead to a large number of switching losses. If the switching loss is reduced by lowering the switching frequency, the CR of the inverter output will increase.

Many studies have been devoted to eliminating the CR of grid-tied inverters. A current ripple compensation technique has been proposed [10]. The error between the average control current

and the reference current was compensated by a certain compensation signal. The problems of inaccuracy inverter output current, average current tracking and current waveform distortion were solved. To minimize line current ripple, each  $60^\circ$  sector was divided into six sub-sectors in [11]. Each sub-sector applied the latest three vectors to ensure the minimum line current ripple. A ripple steering method in [12] was applied to reduce high-frequency CR of the inverter. This method can provide soft switching for power semiconductors.

In addition, researchers have studied the multi-vector FCS-MPC modulation method in [13]. Two or three voltage vectors are applied in each control cycle. It can effectively reduce the CR of inverter output current. Multiple voltage vectors are required for each control cycle in the multi-vector FCS-MPC modulation strategy. The duration of each voltage vector needs to be calculated. There are usually two methods to calculate the duration of each base vector in the multi-vector FCS-MPC strategy. The first is based on the deadbeat control principle [14], while the second is based on the principle that the basic voltage vector is inversely proportional to the duration [15, 16]. Multi-vector MPC modulation can effectively reduce the inverter output CR. However, due to the multi-vector MPC modulation strategy, more than one voltage vector is applied in each control cycle. Compared with the conventional MPC modulation strategy, the inverter switches the switching state more times at the same time. The switching loss is increased.

The ripple of inverter output current is caused by many factors, such as input low-frequency ripples, high-frequency ripples, parasitic parameters and ultra-high frequency resonance noise during power equipment switching. The CR of grid-tied inverters has been regarded as an important research object [17–19]. Although there are many related studies on CR characteristics in [20, 21], an accurate prediction method for real-time CR has not been proposed yet. In [22], a real-time CR prediction method based on a three-level T-type converter was proposed. In [23], a dead-time effect compensation method based on CR prediction for voltage-source inverters was proposed. The CR prediction method in [22, 23] calculates the CR slope through the Thevenin equivalent circuit diagram corresponding to each voltage vector. Finally, the real-time CR is calculated. However, since only one voltage vector is applied in each control cycle in the FCS-MPC strategy, the method by Thevenin's theorem cannot accurately predict the CR in the FCS-MPC strategy. This CR prediction method in [22, 23] is not suitable for the FCS-MPC strategy. In order to solve this problem, this paper improves the conventional CR prediction method for the FCS-MPC strategy.

This paper proposes a current ripple reduction method based on reference current compensation (RCC). In order to realize the reference current compensation, the conventional current ripple prediction method is improved. The improved method uses inverter output voltage and grid voltage to predict current ripples. It makes up for the shortcomings that the conventional current prediction method cannot predict in some switching states. In addition, the differences between two cost functions are compared through visual analysis. It is found that the sensitivity of the square cost function to small errors is better than that of the absolute value function. Finally, the compensated reference current is substituted into the square cost function to reduce the current ripple.

The influence of current ripples on a two-level voltage source inverter is analyzed in section 2. In section 3, the improved CR prediction method is introduced, and the difference between the two cost functions is analyzed by visualization. Section 4 introduces the principle of RCC. Finally, section 5 shows the experimental results.

## 2. Analysis of current ripple using FCS-MPC

This section introduces the structure of two-level voltage source grid-tied inverter and the control principle of the conventional FCS-MPC strategy. In the FCS-MPC strategy, the influence of current ripple on optimal voltage vector selection of two-level voltage source inverter is analyzed.

### 2.1. FCS-MPC strategy for grid-tied inverter

The structure of a three-phase two-level VSI is shown in Fig. 1.  $u_a$ ,  $u_b$  and  $u_c$  are the output voltages of the VSI.  $e_{abc}$  and  $i_{abc}$  are the grid voltages and the inverter output currents, respectively.  $U_{dc}$  is the voltage on the DC side.  $L$  is the filter inductance, and  $R$  is its stray resistance.

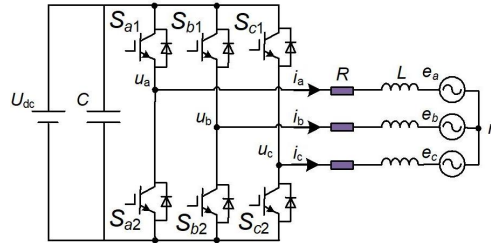


Fig. 1. Structure of two-level voltage source grid-tied inverter

The mathematical model of the two-level VSI in the  $\alpha\beta$  coordinate system can be expressed as

$$\begin{bmatrix} \frac{di_\alpha}{dt} \\ \frac{di_\beta}{dt} \end{bmatrix} = \begin{bmatrix} -\frac{R}{L} & 0 \\ 0 & -\frac{R}{L} \end{bmatrix} \begin{bmatrix} i_\alpha \\ i_\beta \end{bmatrix} + \begin{bmatrix} \frac{1}{L} & 0 \\ 0 & \frac{1}{L} \end{bmatrix} \begin{bmatrix} u_\alpha - e_\alpha \\ u_\beta - e_\beta \end{bmatrix}, \quad (1)$$

where:  $u_\alpha$  and  $u_\beta$  are the output voltages of the two-level VSI,  $i_\alpha$  and  $i_\beta$  are the output currents of the two-level VSI,  $e_\alpha$  and  $e_\beta$  are the grid voltages,  $L$  is the filter inductance and  $R$  is the stray resistance.

As the sampling frequency is much higher than the grid voltage frequency, the discretization of (1) by Euler's forward approximation can approximate the predicted current at the  $(k + 1)$ -th instant. The  $\alpha\beta$  components of the predictive current  $i_\alpha^p$  and  $i_\beta^p$  can be expressed as

$$\begin{bmatrix} i_\alpha^p \\ i_\beta^p \end{bmatrix} = \begin{bmatrix} 1 - \frac{R}{L} & 0 \\ 0 & 1 - \frac{R}{L} \end{bmatrix} \begin{bmatrix} i_\alpha \\ i_\beta \end{bmatrix} + \begin{bmatrix} \frac{T}{L} & 0 \\ 0 & \frac{T}{L} \end{bmatrix} \begin{bmatrix} u_\alpha - e_\alpha \\ u_\beta - e_\beta \end{bmatrix}, \quad (2)$$

where  $T$  is the control period.

Then the cost function  $g$  of conventional FCS-MPC can be given as

$$g = |i_\alpha^* - i_\alpha^p| + |i_\beta^* - i_\beta^p|, \quad (3)$$

where  $i_\alpha^*$  and  $i_\beta^*$  are the reference currents.

The eight predicted currents are substituted into (3). The voltage vector that minimizes the cost function is selected as the optimal vector and applied to the next period.

## 2.2. Influence analysis of current ripple

For constant-switching frequency FCS-MPC, each switch state corresponds to a current ripple. The difference between the DC-link voltage and instantaneous AC-voltage determines the CR.

According to (1), ignoring the effect of the resistance  $R$ , it can be deduced that

$$i_{\alpha\beta}^*(k+1) \approx i_{\alpha\beta}^P(k+1) = i_{\alpha\beta}(k) + \Delta i, \quad (4)$$

where  $\Delta i = T[\mathbf{u}_{\alpha\beta}(k) - \mathbf{e}_{\alpha\beta}(k)]/L$ ,  $\mathbf{u}_{\alpha\beta} = [u_\alpha, u_\beta]^T$  and  $\mathbf{e}_{\alpha\beta} = [e_\alpha, e_\beta]^T$ .  $i_{\alpha\beta}^*(k+1)$  is the reference current at the  $(k+1)$ -th instant.

According to (4), the current error  $\Delta i$  can be expressed as

$$\Delta i \approx i_{\alpha\beta}^P(k+1) - i_{\alpha\beta}(k) = \Delta i^*. \quad (5)$$

When  $\Delta i$  depends on  $\mathbf{u}_{\alpha\beta}(k)$  and  $\mathbf{e}_{\alpha\beta}(k)$  in the  $\alpha\beta$  coordinate system, the amplitude of  $\Delta i$  is constant and the phase is consistent with  $i_{\alpha\beta}^P(k+1)$ . The amplitude and phase of  $\Delta i$  are consistent with  $\Delta i$  by selecting  $u_{\alpha\beta}(k)$ .

Due to the influence of switching characteristics, the actual output voltage of the inverter cannot reach the theoretical value. As shown in Fig. 2,  $u_{\text{out}}$  represents the actual output voltage of the inverter, and  $\Delta u$  represents the fluctuating voltage across the inductor. The time  $d$ , during which the optimal voltage vector acts in each cycle, can be expressed as

$$d = \frac{T}{2} \left( 1 + \frac{u_m}{U_{\text{tri}}} \right), \quad (6)$$

where  $u_m$  is the modulation amplitude and  $U_{\text{tri}}$  represents the triangular carrier amplitude.

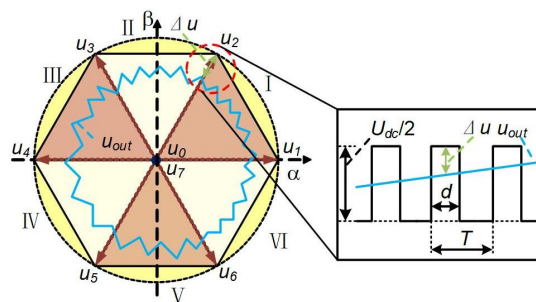


Fig. 2. Analysis of current ripple influence

The fluctuating current  $\Delta i_L$  through the inductance of the filter in the time  $d$  is expressed as

$$\begin{aligned} \Delta i_L &= \frac{\Delta u}{L} d = \frac{\frac{U_{dc}}{2} - u_o}{L} \times \frac{T}{2} \times \frac{U_{tri} + u_m}{U_{tri}} \\ &= \frac{\frac{U_{dc}}{2} - \frac{u_m}{U_{tri}} \cdot \frac{U_{dc}}{2}}{L} \times \frac{T}{2} \times \frac{U_{tri} + u_m}{U_{tri}} = \frac{U_{dc} T (U_{tri}^2 - u_m^2)}{4 L U_{tri}^2}. \end{aligned} \quad (7)$$

According to (7), when the optimal voltage vector is applied at the  $(k + 1)$ -th instant, there is an error  $\Delta i_L$  between the actual output current and ideal output current. The FCS-MPC strategy selects the optimal vector by comparing each voltage vector with the reference value. The cost function includes not only the difference between the predicted value and the reference value, but also the error between actual output value and ideal output value.

As only one voltage vector is applied in every control period in the conventional FCS-MPC strategy, the CR is large. The CR affects the selection of the optimal voltage vector. In order to suppress the CR, it is necessary to predict the real-time CR. First, the influence of current ripples on the optimal voltage vector selection in the conventional MPC strategy is analyzed. Then, the conventional current ripple prediction method is improved to make it more suitable for the MPC strategy.

### 3. Proposed current ripple prediction method for FCS-MPC strategy

#### 3.1. Proposed current ripples prediction

Taking a two-level VSI as an example, the structure is shown in Fig. 1. According to the inverter output voltage and grid voltage, the inverter output current in one control cycle is calculated, as shown in (8).

$$\mathbf{i}(t) = \mathbf{i}(t_0) \cdot e^{\mathbf{A}(t-t_0)} + \int_{t_0}^t e^{\mathbf{A}(t-\tau)} \mathbf{B}u(\tau) d\tau = \mathbf{i}(t_0) \cdot e^{\mathbf{A}(t-t_0)} + \frac{\mathbf{B}u}{\mathbf{A}} (e^{\mathbf{A}t} - 1), \quad (8)$$

where:  $\mathbf{A} = \text{diag}(-R/L, -R/L)$ ,  $\mathbf{B} = \text{diag}(1/L, 1/L)$ ,  $t - t_0 = T$ ,  $\mathbf{i}(t) = [i_\alpha(t) \ i_\beta(t)]^T$ ,  $i_\alpha(t)$  and  $i_\beta(t)$  are the output currents of the inverter at the  $t$  instant in the  $\alpha\beta$ -axis,  $\mathbf{i}(t_0) = [i_\alpha(t_0) \ i_\beta(t_0)]^T$ ,  $i_\alpha(t_0)$  and  $i_\beta(t_0)$  are the output currents of the inverter at the  $t_0$  instant in the  $\alpha\beta$ -axis.

According to (8), the output current of the inverter at the  $k$ -th instant can be represented by

$$\begin{bmatrix} i_\alpha(k+1) \\ i_\beta(k+1) \end{bmatrix} = \begin{bmatrix} i_\alpha(k) \\ i_\beta(k) \end{bmatrix} e^{-\frac{R}{L}T} + \frac{1 - e^{-\frac{R}{L}T}}{R} \begin{bmatrix} u_\alpha(k) - e_\alpha(k) \\ u_\beta(k) - e_\beta(k) \end{bmatrix}. \quad (9)$$

According to the above analysis, the CR is expressed as

$$\begin{bmatrix} i_{\alpha\_rip}^p \\ i_{\beta\_rip}^p \end{bmatrix} = \begin{bmatrix} i_\alpha(k+1) \\ i_\beta(k+1) \end{bmatrix} - \begin{bmatrix} i_\alpha(k) \\ i_\beta(k) \end{bmatrix} = \begin{bmatrix} i_\alpha(k) \\ i_\beta(k) \end{bmatrix} (e^{-\frac{R}{L}T} - 1) + \frac{1 - e^{-\frac{R}{L}T}}{R} \begin{bmatrix} u_\alpha(k) - e_\alpha(k) \\ u_\beta(k) - e_\beta(k) \end{bmatrix}. \quad (10)$$

The proposed CR prediction method for the FCS-MPC strategy of grid-tied inverters makes up for the shortcomings of the conventional CR prediction method that the CR cannot predict in some switching states. The proposed method calculates the real-time CR by  $i_{\alpha\beta}(k)$ ,  $u_{\alpha\beta}(k)$  and  $e_{\alpha\beta}(k)$ . It is not necessary to calculate the CR slopes under each voltage vector through Thevenin's equivalent circuit.

### 3.2. Visualization of cost function

In the conventional FCS-MPC modulation strategy, the cost function is mainly divided into two types. One is the absolute value of the difference between the reference value and the predicted current value. This type of cost function is collectively referred to as type A in this paper, and it is given by

$$g_1 = |i_{\alpha}^* - i_{\alpha}^p| + |i_{\beta}^* - i_{\beta}^p|. \quad (11)$$

The other is the sum of the difference square between the reference value and the predicted current value. In this paper, this kind of value function is called type B, which leads to

$$g_2 = \begin{bmatrix} i_{\alpha}^* - i_{\alpha}^p & i_{\beta}^* - i_{\beta}^p \end{bmatrix} \begin{bmatrix} i_{\alpha}^* - i_{\alpha}^p & i_{\beta}^* - i_{\beta}^p \end{bmatrix}^T. \quad (12)$$

The cost function  $g_1$  is less stable than the cost function  $g_2$  [24]. According to [25] and [26], the output current error of the cost function  $g_1$  is greater than  $g_2$ .

In order to display the change trend of the two cost functions, the partial derivatives of  $u_{\alpha}$  and  $u_{\beta}$  are calculated for the two cost functions, respectively. The gradient of  $g_1$  (named  $\nabla g_1$ ) is written as

$$\nabla g_1(u_{\alpha}, u_{\beta}) = \left( \frac{\partial g_1}{\partial u_{\alpha}} \quad \frac{\partial g_1}{\partial u_{\beta}} \right)^T = \left( -|i_{\alpha}^* - i_{\alpha}^p| \frac{\partial i_{\alpha}^p}{\partial u_{\alpha}} \quad -|i_{\beta}^* - i_{\beta}^p| \frac{\partial i_{\beta}^p}{\partial u_{\beta}} \right)^T. \quad (13)$$

The gradient of the  $g_1$  (named  $\nabla g_2$ ) cost function is expressed as

$$\nabla g_2(u_{\alpha}, u_{\beta}) = \left( \frac{\partial g_2}{\partial u_{\alpha}} \quad \frac{\partial g_2}{\partial u_{\beta}} \right)^T = \left( -2(i_{\beta}^* - i_{\beta}^p) \frac{\partial i_{\alpha}^p}{\partial u_{\alpha}} \quad -2(i_{\alpha}^* - i_{\alpha}^p) \frac{\partial i_{\beta}^p}{\partial u_{\beta}} \right)^T. \quad (14)$$

The difference between the two types of cost functions shown in Fig. 3 and Fig. 4 is obtained by the method of visualized analysis.

Figure 3(a) and Fig. 4(a) represent the cost function values of type A and B under different reference currents, respectively. Figure 3(b) and Fig. 4(b) represent the trend and isoline of the corresponding cost function changes, respectively. It can be seen that the type A cost function (named  $g_1$ ) changes relatively smoothly and is relatively sensitive to different errors. The type B cost function (named  $g_2$ ) is more sensitive to large errors. When the error is less than 0.4,  $g_2$  changes slowly.

In order to analyze the effects of the two cost functions more specifically, a cost function error  $\delta$  is defined as

$$\delta = \min |i_{\alpha}^* - i_{\alpha}^p| + |i_{\beta}^* - i_{\beta}^p| - \min \begin{bmatrix} i_{\alpha}^* - i_{\alpha}^p & i_{\beta}^* - i_{\beta}^p \end{bmatrix} \begin{bmatrix} i_{\alpha}^* - i_{\alpha}^p & i_{\beta}^* - i_{\beta}^p \end{bmatrix}^T. \quad (15)$$

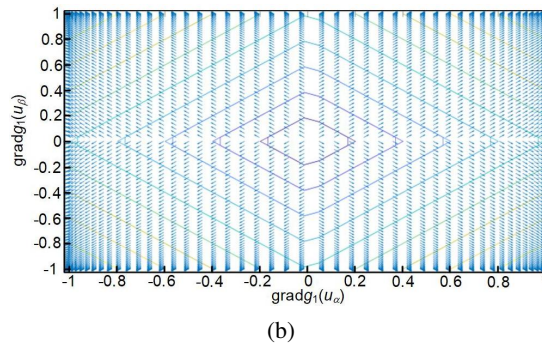
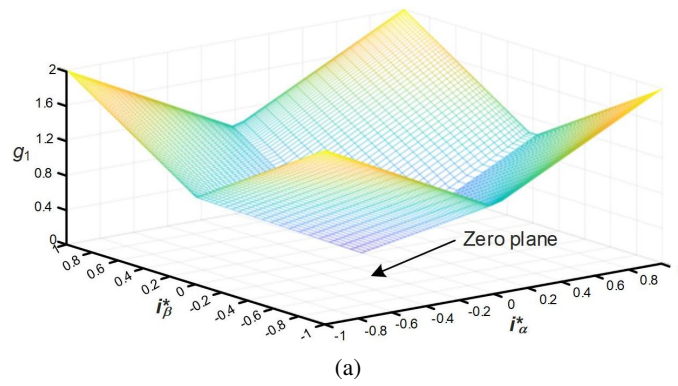


Fig. 3. Type A visual analysis graphs of cost function and gradient map: (a) visual analysis graphs; (b) gradient map

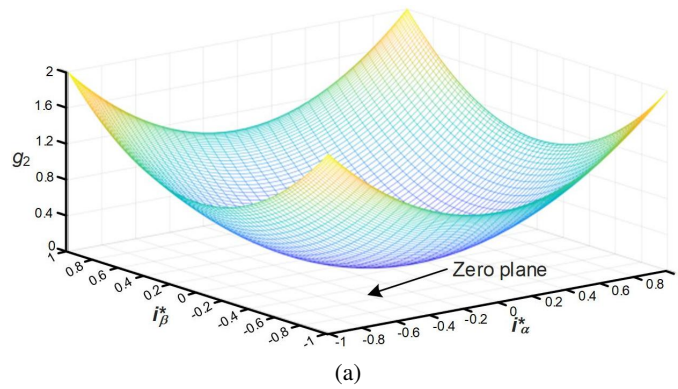


Fig. 4. Type B visual analysis graphs of cost function and gradient map: (a) visual analysis graphs

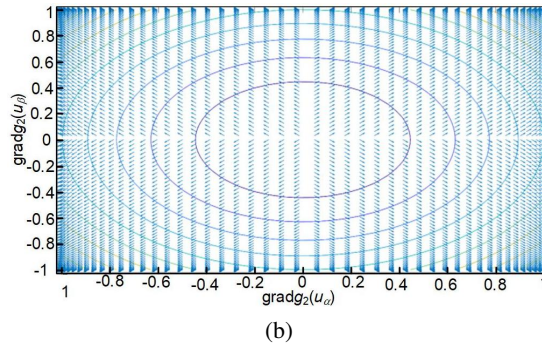


Fig. 4. Type B visual analysis graphs of cost function and gradient map: (a) visual analysis graphs; (b) gradient map

The three-dimensional graph of the error  $\delta$  is shown in Fig. 5.  $\delta$  is greater than or equal to 0 throughout the three-dimensional graph, which means that  $g_2$  is always smaller than  $g_1$  for different basic voltage vectors. Therefore, it can be concluded that the type B cost function is more effective in reducing the control error than the type A cost function. For small errors, the sensitivity can be improved by the RCC method proposed in this paper. The optimal voltage vector is accurately selected without the influence of the CR.

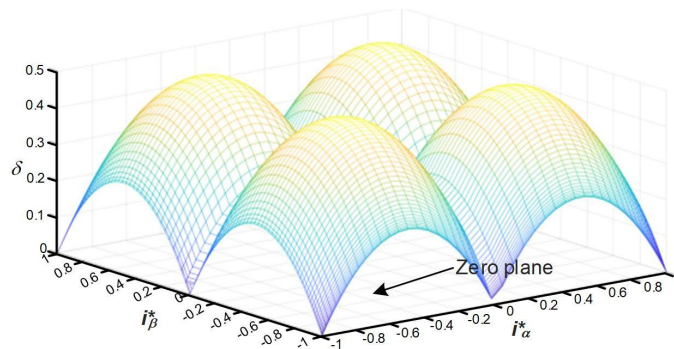


Fig. 5. Three-dimensional graph of two cost functions error  $\delta$

According to the above analysis, the difference between type A and B cost functions are summarized.

1. According to Fig. 3(b) and Fig. 4(b), the type A cost function is more sensitive to small errors. The type B cost function is more sensitive to large errors.
2. According to Fig. 5, the error of the type B cost function is smaller than the errors of type A.

The type B cost function is selected to reduce the control error. The RCC method is used to improve its sensitivity to small errors.

#### 4. Reference current compensation method of FCS-MPC strategy grid-tied inverter

According to the above analysis, the CR in certain areas of the sector has a great influence on vector selection. The inverter output CR causes the inaccurate selection of some optimal voltage vectors. As a result, the THD of the output current waveform is larger. In order to eliminate the influence of the CR on the selection of voltage vectors, the CR suppression method based on RCC is proposed in this paper. By predicting the real-time CR at the  $(k + 1)$ -th instant, the reference current is corrected in advance to compensate for the impact of the CR. The voltage vector predicted based on the reference current after compensation can better fit the reference current before compensation. The schematic diagram of RCC is depicted in Fig. 6. The influence caused by the CR can be effectively compensated. The compensated formula for the reference current is given in (16).

$$\begin{bmatrix} i_{\alpha\_com}^* \\ i_{\beta\_com}^* \end{bmatrix} = \begin{bmatrix} i_{\alpha}^* \\ i_{\beta}^* \end{bmatrix} - \begin{bmatrix} i_{\alpha\_rip}^p \\ i_{\beta\_rip}^p \end{bmatrix}, \quad (16)$$

where:  $i_{\alpha\beta\_com}^* = [i_{\alpha\_com}^*, i_{\beta\_com}^*]^T$ ,  $i_{\alpha\_com}^*$  and  $i_{\beta\_com}^*$  stand for the component of the compensated reference current in the  $\alpha\beta$ -axis.

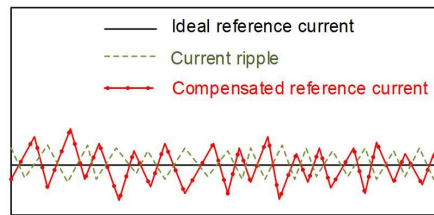


Fig. 6. Reference current compensation diagram

The cost function is obtained by substituting the compensated reference current into the type B cost function. The cost function is

$$g = \begin{bmatrix} i_{\alpha\_com}^* - i_{\alpha}^p & i_{\beta\_com}^* - i_{\beta}^p \end{bmatrix} \begin{bmatrix} i_{\alpha\_com}^* - i_{\alpha}^p & i_{\beta\_com}^* - i_{\beta}^p \end{bmatrix}^T. \quad (17)$$

The control schematic of the proposed RCC method is shown in Fig. 7. The flow chart of the proposed RCC method is shown in Fig. 8.

- Step 1: Collect the grid side voltage  $e(k)$  and three-phase output currents of the two-level VSI  $i(k)$ .
- Step 2: Predict the output current  $i_{\alpha\beta}^p$  and the real-time CR  $i_{\alpha\beta\_rip}^p$  of the inverter under each voltage vector, respectively.
- Step 3: Compensate the reference current based on the predicted current ripple.
- Step 4: The compensated reference current  $i_{\alpha\beta\_com}^*$  is substituted for the original reference current  $i_{\alpha\beta}^*$  to construct a cost function.
- Step 5: Calculate the cost function  $g$  and select the optimal voltage vector.

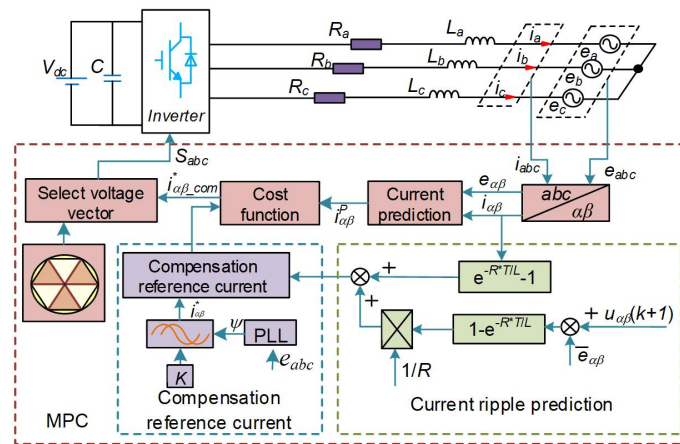


Fig. 7. Control schematic of the proposed reference current compensation

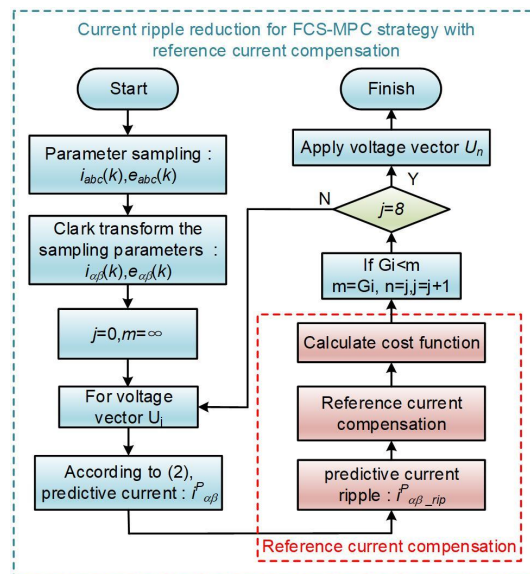


Fig. 8. Algorithm flow chart of the proposed method

The proposed method reduces the CR by compensating the reference current for the FCS-MPC strategy of grid-tied inverters. First, the real-time CR is predicted by inverter output current, inverter output voltage and grid voltage. Then, the reference current is compensated by the predicted real-time CR. The basic control principle of the proposed method is similar to the conventional MPC strategy. So, the proposed control method belongs to open-loop optimal control. The stability of MPC has been verified in detail in [27]. This paper does not give detailed proof.

Table 1 shows the effect comparison of different control methods. It can be seen from Table 1 that the double-vector in [16] and triple-vector MPC in [28] are multiple voltage vectors in a control period. The CR is reduced by improving the accuracy of predicted value. But its switching frequency also increases. The proposed method reduces the CR from the perspective of reference value. Switching frequency will not increase.

Table 1. Comparison between the proposed method and multi-vector MPC strategy

	<b>Conventional MPC</b>	<b>Double-vector MPC</b>	<b>Triple-vector MPC</b>	<b>Proposed method</b>
Current ripple	large	Smaller	Small	Smaller
Voltage vector in each control period	1	2	3	1
Switching frequency	Low	Medium	High	Low
Algorithm calculation burden	Small	Medium	Large	Medium

According to the above analysis, the conclusions for CR reduction for the FCS-MPC strategy of grid-tied inverters with RCC can be drawn as follows:

1. The CR will affect the selection of the optimal voltage vector at the next instant in the FCS-MPC strategy.
2. The influence of the CR on the selection of the optimal vector can be eliminated by compensating the reference current.

## 5. Experimental results

In order to verify the effectiveness of the proposed method, the experimental waveforms are illustrated in this section. The experiment platform for a two-level voltage source grid-tied inverter is shown in Fig. 9. The main control chip of the inverter is DSP28335. The parameters are shown in Table 2.

Table 2. Experimental parameters

<b>Parameter name</b>	<b>Symbol</b>	<b>Value</b>	<b>Unit</b>
DC voltage	$U_{dc}$	250	V
Peak of grid line voltage	$e$	150	V
Filter inductance	$L$	10	mH
Parasitic resistance	$R$	50	m $\Omega$
Grid frequency	$f$	50	Hz
Sampling frequency	$f_s$	10	kHz

Experimental waveforms include static experimental waveforms and dynamic experimental waveforms. The steady-state experiment includes the comparison of inverter output current and parameters mismatch experiments. The dynamic experiment includes inverter output current and the current CR when the reference current changes from 6 A to 10 A.

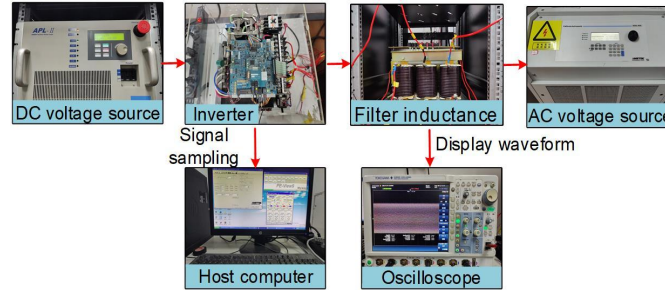


Fig. 9. Experiment platform of two-level voltage source grid-tied inverter

### 5.1. Steady state experimental results

In Fig. 10, the CR of the proposed method is compared with that of the conventional FCS-MPC strategy. When the reference current is 10 A, the maximum CR of the conventional FCS-MPC strategy is 1.9 A. The maximum CR is reduced to 1 A. The amplitude and effective value of the real-time CR are reduced. The variation of output current before and after the ripple at the peak is more obvious. The THD of the conventional FCS-MPC is 3.86%. After adopting the proposed method, the THD is reduced to 2.96%. According to the data of the analysis experiment, the higher harmonic content of the inverter output current is suppressed after using the proposed method.

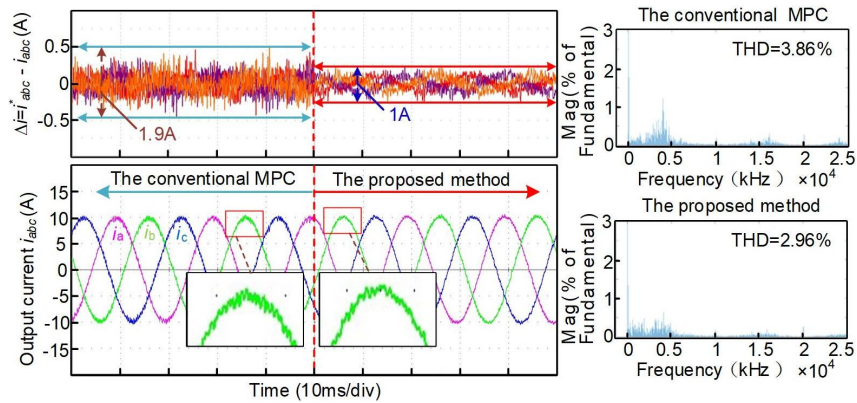


Fig. 10. Inverter output current and current error

Figure 11 shows the THDs under different reference currents. It can be concluded that the proposed method can reduce the current THD under different reference currents.

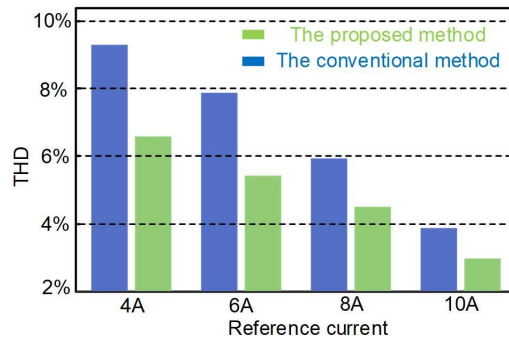


Fig. 11. The current THDs with different currents

In order to verify the robustness of the proposed method to parameter variations, the experimental study is carried out with inaccurate model parameters. The actual inductance in the inverter is 10 mH. Two experiments are carried out according to the parameters set in [14]. The inductance value in the controller is greater (20 mH) or less (5 mH) than the actual inductance value. The experimental results are shown in Fig. 12 and Fig. 13.

It can be seen from Fig. 12 that when the inductance in the controller is greater than the actual inductance, the CR becomes larger. The proposed method has an obvious effect on ripple suppression.

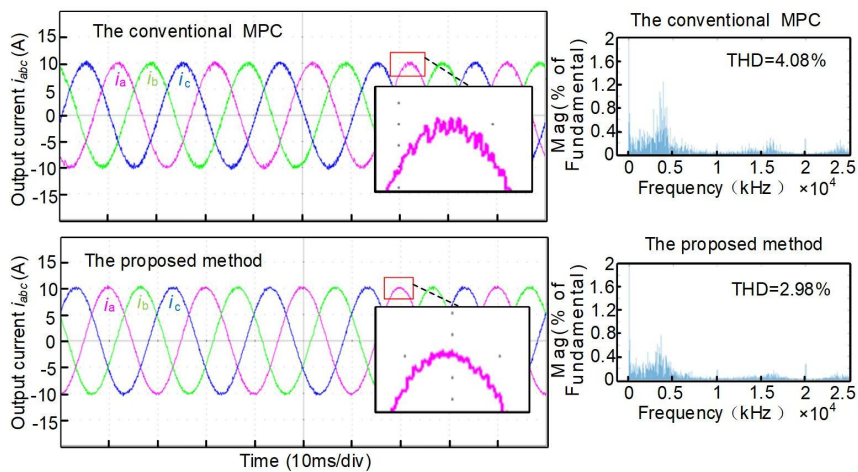


Fig. 12. Inverter output current when the inductance in the controller is 20 mH

It can be seen from Fig. 13 that when the inductance in the controller is smaller than the actual inductance, the current waveform is distorted. The effect of the proposed method on CR suppression is weakened. But the proposed method is still effective when the parameters are mismatched.

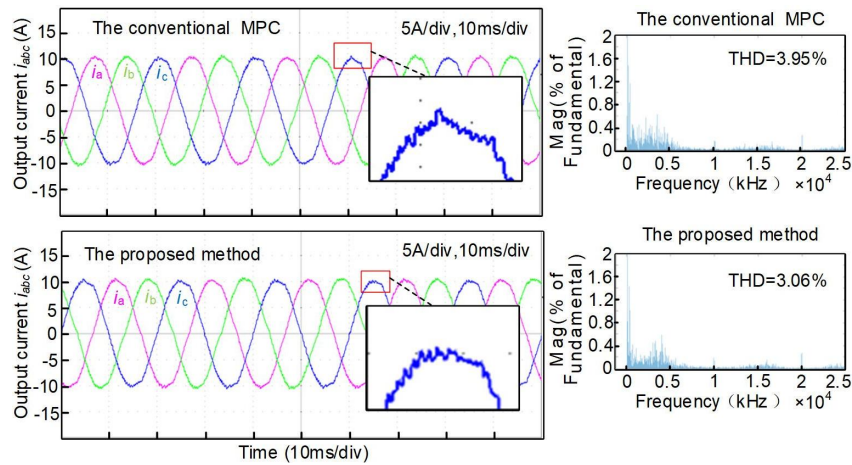


Fig. 13. Inverter output current when the inductance in the controller is 5 mH

## 5.2. Dynamic state experimental results

The performance of the proposed method is further verified by dynamic experiments. Figure 14 shows the dynamic three-phase current waveform and CR of phase a when the reference current changes from 6 A to 10 A.

When the reference current changes from 6 A to 10 A, the inverter output current can quickly track the change of the reference current. The inverter output current error does not increase with the change of the reference current. When the reference current is 6 A, the THD is 4.25%. When the reference current increases to 10 A, THD decreases to 2.96%. The amplitude of the inverter output CR remains at 1 A. The proposed method does not show the overshoot phenomenon, which further verifies the effectiveness of the proposed method.

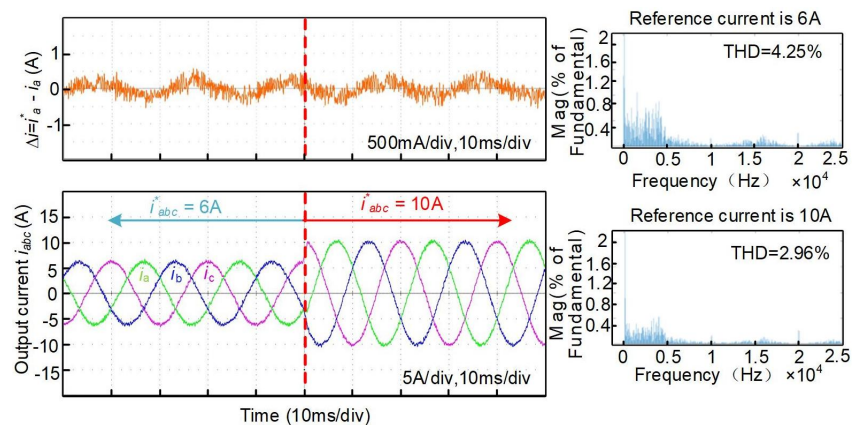


Fig. 14. Dynamic experimental results of the proposed method when three-phase current rises from 6 A to 10 A

## 6. Conclusions

The conventional FCS-MPC strategy of the voltage source grid-tied inverter can be affected by the CR when selecting the optimal voltage vector and lead to an inaccurate selection of the optimal voltage vector. This paper analyzes the influence of current ripples on the optimal voltage vector selection of a two-level voltage source inverter. The current ripple prediction method is improved. The improved method uses inverter output voltage and grid voltage to calculate current ripples based on the space state equation. It makes up for the shortcomings that the conventional current prediction method cannot predict in some switching states. The improved current ripple predictive method is more suitable for the FCS-MPC strategy. In addition, the differences between the two cost functions are compared through visual analysis. It is found that the sensitivity of the square cost function to small errors is better than that of the absolute value function. Finally, the predicted current ripple is used to compensate the reference current. The current ripple is reduced by compensating the reference current.

The experimental results show that the proposed method is effective for two-level voltage source inverters. However, the feasibility of the proposed reference current compensation method in other inverter structures can also be studied, for example, in a T-type inverter and NPC (Neutral Point Clamped) three-level inverter. In the future, we will study the application of the proposed reference current compensation method in other structural inverters.

### Acknowledgements

This research was supported in part by the National Nature Science Foundation of China under Grant U2004166, in part by the Province Key Research and Development and Promotion of Special Projects (Science and Technology) Grant 222102210059, and in part by Science and Technology Innovation Team in Universities of Henan Province under Grant 22IRTSTHN017.

### References

- [1] Jayalakshmi N.S., Gaonkar D.N., Karthik R.P., Prasanna P., *Intermittent power smoothing control for grid connected hybrid wind/PV system using battery-EDLC storage devices*, Archives of Electrical Engineering, vol. 69, no. 2, pp. 433–453 (2020), DOI: [10.24425/ae.2020.133036](https://doi.org/10.24425/ae.2020.133036).
- [2] Sun K., Wang X.S., Li Y.W., Nejabatkhah F., Yang M., Lu X., *Parallel operation of bidirectional interfacing converters in a hybrid AC/DC microgrid under unbalanced grid voltage conditions*, IEEE Transactions on Power Electronics, vol. 32, no. 3, pp. 1872–1884 (2017), DOI: [10.1109/TPEL.2016.2555140](https://doi.org/10.1109/TPEL.2016.2555140).
- [3] Vekhande V., Kanakesh V.K., Fernandes B.G., *Control of three-phase bidirectional current-source converter to inject balanced three-phase currents under unbalanced grid voltage condition*, IEEE Transactions on Power Electronics, vol. 31, no. 9, pp. 6719–6737 (2016), DOI: [10.1109/TPEL.2015.2503352](https://doi.org/10.1109/TPEL.2015.2503352).
- [4] Li H., Xiao H., Yang G., *Reconstructed current model predictive control of NPC three-level grid-tied converter with current sensor fault*, IEEE Access, vol. 9, pp. 141098–141106 (2021), DOI: [10.1109/ACCESS.2021.3119566](https://doi.org/10.1109/ACCESS.2021.3119566).
- [5] Guo L., Jin N., Gan C., Luo K., *Hybrid voltage vector preselection-based model predictive control for two-level voltage source inverters to reduce the common-mode voltage*, IEEE Transactions on Industrial Electronics, vol. 67, no. 6, pp. 4680–4691 (2020), DOI: [10.1109/TIE.2019.2931257](https://doi.org/10.1109/TIE.2019.2931257).

- [6] Estévez-Bén Adyr A., Alfredo Alvarez-Diazcomas, Juvenal Rodriguez Reséndiz, *Transformerless Multilevel Voltage-Source Inverter Topology Comparative Study for PV Systems*, *Energies*, vol. 13, no. 12 (2020), DOI: [10.3390/en13123261](https://doi.org/10.3390/en13123261).
- [7] Héctor López, Nimrod Vázquez, Juvenal Rodriguez *et al.*, *Analysis and implementation of a finite-control-set by using model solution-based control for three-phase VSI*, *IET Power Electronics*, vol. 10, no. 14, pp. 1832–1840 (2017), DOI: [10.1049/iet-pe.2016.0819](https://doi.org/10.1049/iet-pe.2016.0819).
- [8] Estévez-Bén Adyr A. *et al.*, *A new predictive control strategy for multilevel current-source inverter grid-connected*, *Electronics*, vol. 8, no. 8 (2019), DOI: [10.3390/electronics8080902](https://doi.org/10.3390/electronics8080902).
- [9] Tang M., Yang S., Zhang K. *et al.*, *Model predictive direct power control of energy storage quasi-Z-source grid-connected inverter*, *Archives of Electrical Engineering*, vol. 71, no. 1, pp. 21–35 (2022), DOI: [10.24425/ae.2022.140195](https://doi.org/10.24425/ae.2022.140195).
- [10] Lu W., Li S., Chen W., *Current-ripple compensation control technique for switching power converters*, *IEEE Transactions on Industrial Electronics*, vol. 65, no. 5, pp. 4197–4206 (2018), DOI: [10.1109/TIE.2017.2762622](https://doi.org/10.1109/TIE.2017.2762622).
- [11] Zeng Z., Li Z., Goetz S.M., *Line current ripple minimization PWM strategy with reduced zero-sequence circulating current for two parallel interleaved three-phase converters*, *IEEE Transactions on Power Electronics*, vol. 35, no. 7, pp. 6931–6943 (2020), DOI: [10.1109/TPEL.2019.2958878](https://doi.org/10.1109/TPEL.2019.2958878).
- [12] Samani R., Beyragh D.S., Pahlevani M., *A new grid-connected DC/AC inverter with soft switching and low current ripple*, *IEEE Transactions on Power Electronics*, vol. 34, no. 5, pp. 4480–4496 (2019), DOI: [10.1109/TPEL.2018.2863183](https://doi.org/10.1109/TPEL.2018.2863183).
- [13] Zhang Y., Jiang H., Yang H., *Model predictive control of PMSM drives based on a general discrete space vector modulation*, *IEEE Transactions on Energy Conversion*, vol. 36, no. 2, pp. 1300–1307 (2021), DOI: [10.1109/TEC.2020.3036082](https://doi.org/10.1109/TEC.2020.3036082).
- [14] Liu T., Chen A., Qin C., Chen J., Li X., *Double vector model predictive control to reduce common-mode voltage without weighting factors for three-level inverters*, *IEEE Transactions on Industrial Electronics*, vol. 67, no. 10, pp. 8980–8990 (2020), DOI: [10.1109/TIE.2020.2994876](https://doi.org/10.1109/TIE.2020.2994876).
- [15] Cao L.Z., Li Y.Y., Li X.Y., Guo L.L., Jin N., Cao H., *A dual-vector modulated model predictive control method for voltage source inverters with a new duty cycle calculation method*, *Energies*, vol. 13, no. 16, pp. 9204–9214 (2020), DOI: [10.3390/en13164200](https://doi.org/10.3390/en13164200).
- [16] Jin N., Chen M., Guo L., Li Y., Chen Y., *Double-vector model-free predictive control method for voltage source inverter with visualization analysis*, *IEEE Transactions on Industrial Electronics*, vol. 69, no. 10, pp. 10066–10078 (2022), DOI: [10.1109/TIE.2021.3128905](https://doi.org/10.1109/TIE.2021.3128905).
- [17] Kim S., Won I.J., Kim J., Lee K., *DC-link ripple current reduction method for three-level inverters with optimal switching pattern*, *IEEE Transactions on Industrial Electronics*, vol. 65, no. 12, pp. 9204–9214 (2018), DOI: [10.1109/TIE.2018.2823662](https://doi.org/10.1109/TIE.2018.2823662).
- [18] Lu W., Li S., Chen W., *Current-ripple compensation control technique for switching power converters*, *IEEE Transactions on Industrial Electronics*, vol. 65, no. 5, pp. 4197–4206 (2018), DOI: [10.1109/TIE.2017.2762622](https://doi.org/10.1109/TIE.2017.2762622).
- [19] Zeng Z., Li Z., Goetz S.M., *Line current ripple minimization PWM strategy with reduced zero-sequence circulating current for two parallel interleaved three-Phase converters*, *IEEE Transactions on Power Electronics*, vol. 35, no. 7, pp. 6931–6943 (2020), DOI: [10.1109/TPEL.2019.2958878](https://doi.org/10.1109/TPEL.2019.2958878).
- [20] Cervellini P., Antoszczuk P., Retegui R.G., Funes M., *Current ripple amplitude measurement in multiphase power converters*, *IEEE Transactions on Power Electronics*, vol. 32, no. 9, pp. 6684–6688 (2017), DOI: [10.1109/TPEL.2017.2686784](https://doi.org/10.1109/TPEL.2017.2686784).

- [21] Chang L., Jahns T.M., *Prediction and evaluation of PWM-induced current ripple in IPM machines incorporating slotting, saturation, and cross-coupling effects*, 2017 20th International Conference on Electrical Machines and Systems (ICEMS), Sydney, Australia, pp. 1–6 (2017).
- [22] Wang Z., Zhao Z., Hammad Uddin M., Zhao Y., *Current ripple analysis and prediction for three-level T-type converters*, 2018 IEEE Energy Conversion Congress and Exposition (ECCE), Portland, USA, pp. 7251–7257 (2018).
- [23] Shen Z., Jiang D., *Dead-time effect compensation method based on current ripple prediction for voltage-source inverters*, IEEE Transactions on Power Electronics, vol. 34, no. 1, pp. 971–983 (2019), DOI: [10.1109/TPEL.2018.2820727](https://doi.org/10.1109/TPEL.2018.2820727).
- [24] Karamanakos P., Geyer T., *Guidelines for the Design of Finite Control Set Model Predictive Controllers*, IEEE Transactions on Power Electronics, vol. 35, no. 7, pp. 7434–7450 (2020), DOI: [10.1109/TPEL.2019.2954357](https://doi.org/10.1109/TPEL.2019.2954357).
- [25] Mirzaeva G., Goodwin G., Townsend C., *A simple and effective strategy to reduce switching losses under FS-MPC based on dynamically changing voronoi diagrams*, 2017 12th IEEE Conference on Industrial Electronics and Applications (ICIEA), Siem Reap, Cambodia, pp. 1516–1521 (2017).
- [26] Mirzaeva G., Goodwin G.C., McGrath B., *A new understanding and improvements of finite set model predictive control in inverter applications*, 2015 17th European Conference on Power Electronics and Applications (EPE'15 ECCE-Europe), Geneva, Switzerland, pp. 1–10 (2015).
- [27] Andrew E.T., Ahmed K.H., Holliday D., *A new model predictive current controller for grid connected converters in unbalanced grids*, IEEE Transactions on Power Electronics, vol. 37, no. 8, pp. 9175–9186 (2022), DOI: [10.1109/TPEL.2022.3158016](https://doi.org/10.1109/TPEL.2022.3158016).
- [28] Guo L., Chen M., Li Y., Wang P., Jin N., Wu J., *Hybrid multi-vector modulated model predictive control strategy for voltage source inverters based on a new visualization analysis method*, IEEE Transactions on Transportation Electrification (2022), DOI: [10.1109/TTE.2022.3161583](https://doi.org/10.1109/TTE.2022.3161583).